Geophysical Journal International

Geophys. J. Int. (2014) **198,** 1878–1889 doi: 10.1093/gji/ggu228
GJI Seismology

Models and Fréchet kernels for frequency-(in)dependent Q

Andreas Fichtner and Martin van Driel

Department of Earth Sciences, ETH Zurich, Switzerland. E-mail: andreas.fichtner@erdw.ethz.ch

Accepted 2014 June 16. Received 2014 June 16; in original form 2014 April 14

SUMMARY

We present a new method for the modelling of frequency-dependent and frequency-independent Q in time-domain seismic wave propagation. Unlike previous approaches, attenuation models are constructed such that Q as a function of position in the Earth appears explicitly as a parameter in the equations of motion. This feature facilitates the derivation of Fréchet kernels for Q using adjoint techniques. Being simple products of the forward strain field and the adjoint memory variables, these kernels can be computed with no additional cost, compared to Fréchet kernels for elastic properties. The same holds for Fréchet kernels for the power-law exponent of frequency-dependent Q, that we derive as well. To illustrate our developments, we present examples from regional- and global-scale time-domain wave propagation.

Key words: Tomography; Seismic attenuation; Computational seismology; Theoretical seismology; Wave propagation.

1 INTRODUCTION

Seismic waves propagating through the Earth are attenuated due to a multitude of microscale processes including diffusion and dislocation creep of point defects, grain boundary sliding and the viscous motion in (partially) molten material (e.g. Jackson 2007; Karato 2008, chapter 11). Commonly described macroscopically in terms of the quality factor Q, viscoelastic attenuation leads to seismic phase velocity dispersion and to an amplitude reduction of seismic waves (e.g. Dahlen & Tromp 1998; Kennett 2001; Aki & Richards 2002). Numerous laboratory experiments consistently revealed a temperature and frequency dependence of Q for Earth materials that can be described phenomenologically by the Arrhenius-type equation

$$Q(\omega) = Q_0 \left(\frac{\omega}{\omega_0}\right)^{\alpha} \mathrm{e}^{\alpha E/RT}, \qquad (1)$$

where E is the activation energy, T is temperature, R is the gas constant and ω_0 is a reference frequency (e.g. Goetze 1971; Goetze & Brace 1972; Gueguen *et al.* 1989; Karato & Spetzler 1990; Jackson 2000). Typical values for the constant α, summarized for instance by Karato (2008), range between 0.2 and 0.4. Much of the seismological interest in Q is related to its exponential dependence on T, which suggests that attenuation may serve as a proxy for temperature in the Earth. The frequency dependence of Q found in laboratory studies has been confirmed by analyses of seismic data across the seismologically observable frequency band from $\sim 10^{-3}$ to ~ 1 Hz (e.g. Anderson & Minster 1979; Sipkin & Jordan 1979; Flanagan & Wiens 1998; Cheng & Kennett 2002; Lekić *et al.* 2009). A review on the frequency dependence of Q may be found, for instance, in Romanowicz & Mitchell (2007). Despite convincing evidence for a power-law dependence of Q on frequency, the majority of seismic studies assume frequency-independent attenuation. This simplification can be justified by the sparsity and bandlimited nature of seismic observations that often prevent reliable estimates of α.

With the advent of the numerical age, the proper modelling of seismic wave attenuation has received considerable attention. While the implementation of viscoelastic attenuation in frequency-domain numerical modelling is nearly trivial, attenuation is more difficult to implement in time-domain wave propagation schemes that are most frequently used in large-scale 3-D applications (e.g. Igel *et al.* 1995; Komatitsch & Tromp 1999; Moczo *et al.* 2002; Chen *et al.* 2007; Dumbser *et al.* 2007; Fichtner *et al.* 2009; Tape *et al.* 2010). Following the seminal work of Emmerich & Korn (1987) and Carcione *et al.* (1988a,b), attenuation has been modelled almost exclusively by superpositions of rheological bodies of either Maxwell or Zener type that have been shown to be equivalent (Moczo & Kristek 2005). The discrete ensemble of relaxation meachnisms leads, by construction, to a numerically convenient set of equations (Robertsson *et al.* 1994; Blanch *et al.* 1995; van Driel & Nissen-Meyer 2014a). The rheological bodies are described in terms of relaxation variables that are determined such that a prescribed $Q(\omega)$ is matched as closely as possible. The concept of representing a broad absorption band by a superposition of individual relaxation mechanisms already appears in Liu *et al.* (1976), where it had, however, not been used for numerical modelling.

While the forward problem of viscoelastic wave propagation can be considered solved (at least when sufficient computational resources are available), the inverse problem remains technically challenging because Q does not appear explicitly in the description of

© The Authors 2014. Published by Oxford University Press on behalf of The Royal Astronomical Society.

the rheological bodies used to model attenuation (see Section 2.1.1 for details). Instead, Q is determined implicitly by the set of suitably chosen relaxation parameters. Furthermore, the relation between Q and the relaxation parameters may vary from one location to another. The absence of an explicit Q in the time-domain viscoelastic wave equation complicates the computation of Fréchet kernels that are needed to invert for the heterogeneous distribution of Q in the Earth.

Based on the assumption of a frequency-independent Q, Tromp *et al.* (2005) proposed to circumvent this problem through the definition of additional adjoint sources for the computation of Q kernels. This approach, adopted for instance by Bozdağ *et al.* (2011) and Zhu *et al.* (2013), yields correct kernels, but it also doubles the computational cost because an additional adjoint simulation must be performed. Furthermore, an extension to frequency-dependent Q seems difficult.

Here we present a new approach to the time-domain modelling of viscoelastic wave propagation with frequency-dependent or frequency-independent attenuation where Q at a specified reference frequency appears explicitly in the equations of motion. In addition to improving computational efficiency, this approach allows us to compute Fréchet kernels for Q and its frequency dependence without the requirement of additional wavefield simulations.

This paper is organized as follows. To introduce basic concepts without heavy notation, we start our developments in Section 2.1 using a 1-D scalar wave equation. In Section 2.1.2, we describe a novel parametrization of attenuation models where Q appears explicitly. Subsequently, in Section 2.2 we make the transition to the elastic case. A examples, we consider isotropic media, as well as full anisotropy with 21 independent elastic parameters. Section 3 is dedicated to the derivation of shear and bulk Q kernels, based on the previously derived Q models. In the interest of a readable text, we defer the derivation of kernels for the power-law exponent α to the Appendix. Examples of synthetic seismograms for frequency-dependent Q and corresponding Fréchet kernels are presented in Section 4.

2 FORWARD MODELLING

2.1 The scalar wave equation

For the purpose of illustration, we start our development with the scalar wave equation. Written in velocity–stress formulation, it consists of the momentum conservation law

$$\rho \dot{v} - \partial_x \sigma = f, \tag{2}$$

and the viscoelastic constitutive relation defined by

$$\dot{\sigma}(t) = \int_{-\infty}^{\infty} \dot{C}(t - t')\dot{\epsilon}(t')\,\mathrm{d}t' . \tag{3}$$

In eq. (3), σ, C and $\epsilon = \partial_x v$ are representative components of the stress tensor $\boldsymbol{\sigma}$, the elastic tensor $\mathbf{C}$ and the strain tensor $\boldsymbol{\epsilon}$, respectively.

2.1.1 Numerical modelling of viscoelastic attenuation

Taking inspiration from Blanch *et al.* (1995), we model the time-dependence of the elastic modulus C by a superposition of $N \geq 1$ exponential functions with decay times τ_p ($p = 1, \ldots, N$) that phenomenologically mimick different relaxation mechanisms in the Earth:

$$C(t) = C^r \left[1 + \tau \sum_{p=1}^{N} D^{(p)} \mathrm{e}^{-t/\tau^{(p)}} \right] H(t) . \tag{4}$$

The symbol C^r denotes the relaxed modulus, $D^{(p)}$ are the weights of the relaxation mechanisms, H is the Heaviside function and τ is a parameter that controls the strength of viscoelastic attenuation. As described in Section 2.1.2, the free parameters $D^{(p)}$, $\tau^{(p)}$ and τ must be determined such that $C(t)$ approximates a pre-defined behaviour. Differentiating (4) with respect to time t, and introducing the result into (3), yields

$$\dot{\sigma} = C^r (1 + s\tau)\,\dot{\epsilon} + C^r \tau \sum_{p=1}^{N} M^{(p)} , \quad \text{with} \quad s = \sum_{p=1}^{N} D^{(p)} , \tag{5}$$

where the memory variables

$$M^{(p)}(t) = -\frac{D^{(p)}}{\tau^{(p)}} \int_{-\infty}^{\infty} \mathrm{e}^{-(t-t')/\tau^{(p)}} H(t - t')\dot{\epsilon}(t')\,\mathrm{d}t' \tag{6}$$

satisfy the first-order differential equation

$$\dot{M}^{(p)} = -\frac{D^{(p)}}{\tau^{(p)}} \dot{\epsilon} - \frac{1}{\tau^{(p)}} M^{(p)} . \tag{7}$$

The combination of eq. (7), the momentum conservation law (2), and the constitutive relation (3), forms a complete set of equations that describes the propagation of a scalar viscoelastic wave.

2.1.2 Constructing Q models

The quality factor $Q(\omega)$ is defined as the ratio

$$Q(\omega) = \frac{\mathrm{Re}\, C(\omega)}{I C(\omega)} , \tag{8}$$

where the complex modulus $C(\omega)$ is given by

$$C(\omega) = \mathrm{i}\omega \int_{-\infty}^{\infty} C(t)\mathrm{e}^{-\mathrm{i}\omega t}\,\mathrm{d}t . \qquad (i = \sqrt{-1}). \tag{9}$$

When Q is sufficiently large, typically $\gtrsim$100, it can be related to the fractional energy loss per oscillation cycle, that is $\Delta E/E = -2\pi Q^{-1}$. For the specific form of $C(t)$ defined in eq. (4), we find

$$Q(\omega) = \left[1 + \tau \sum_{p=1}^{N} \frac{D^{(p)}\omega^2\tau^{(p)2}}{1 + \omega^2\tau^{(p)2}} \right] \left[\tau \sum_{p=1}^{N} \frac{D^{(p)}\omega\tau^{(p)}}{1 + \omega^2\tau^{(p)2}} \right]^{-1} . \tag{10}$$

To construct Q-models that approximate a prescribed empirical frequency dependence of the form suggested already in eq. (1),

$$Q_{\mathrm{target}}(\omega) = Q_0 \left(\frac{\omega}{\omega_0} \right)^{\alpha} \tag{11}$$

across the frequencies of interest, we proceed as follows:

(i) We define a set of Q_0 values, $(Q_0^{(1)}, \ldots, Q_0^{(M)})$, that span the range of Q in our earth model.

(ii) We set $\tau = Q_0^{(k)}$ for each $k = 1, \ldots, M$. This defines a collection of numerical Q models, $Q(\omega, Q_0^{(k)})$, via eq. (10).

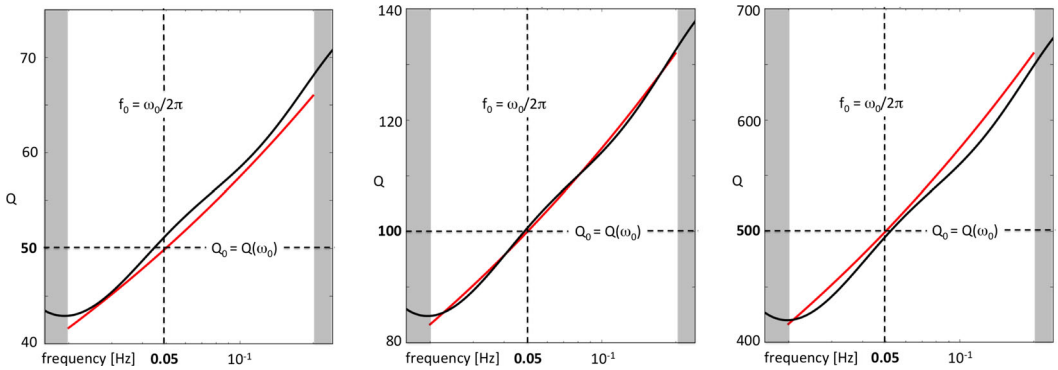

Figure 1. Black curves show $Q(\omega)$ for Q_0 equal to 50, 100 and 500 (from left- to right-hand side) for $N = 3$ relaxation mechanisms. $Q_{\text{target}}(\omega) = Q_0(\omega/\omega_0)^{\alpha}$ with $\alpha = 0.3$ and $\omega_0 = 2\pi \cdot 0.05$ Hz is shown in red. The optimal relaxation times and weights are $\tau_1 = 0.14$, $\tau_2 = 1.40$ s, $\tau_3 = 9.46$ s, $D_1 = 1.23$, $D_2 = 0.91$ and $D_3 = 2.07$. Within the target frequency range 0.02–0.2 Hz, $Q(\omega)$ matches $Q_{\text{target}}(\omega)$ to within 3 per cent of the respective Q_0.

(iii) We find optimal values for $\tau^{(p)}$ and $D^{(p)}$ by minimizing the cumulative difference between the numerical Q models $Q(\omega, Q_0^{(k)})$ and the target Q models $Q_{\text{target}}(\omega, Q_0^{(k)})$,

$$\mathcal{J}(\tau_p, D_p) = \sum_{k=1}^{M} || \, [Q(\omega, Q_0^{(k)}) - Q_{\text{target}}(\omega, Q_0^{(k)})]/Q_0^{(k)} \, ||_{\omega} \, . \quad (12)$$

The minimization of $\mathcal{J}$ represents a non-linear optimization problem in a low-dimensional parameter space that can be solved efficiently with Monte Carlo-type techniques . Finding optimal τ_p and D_p for a whole set of Q_0 values has the effect that the approximation

$$Q(\omega) = \left[1 + Q_0^{-1} \sum_{p=1}^{N} \frac{D^{(p)} \omega^2 \tau^{(p)2}}{1 + \omega^2 \tau^{(p)2}} \right] \left[Q_0^{-1} \sum_{p=1}^{N} \frac{D^{(p)} \omega \tau^{(p)}}{1 + \omega^2 \tau^{(p)2}} \right]^{-1}$$
$$\approx Q_0 \left(\frac{\omega}{\omega_0} \right)^{\alpha} \quad (13)$$

effectively holds for any Q_0 inside the range of Q's in the earth model. The proposed optimization scheme for the relaxation parameters $\tau^{(p)}$ and $D^{(p)}$ explicitly introduces Q_0 into the equations of motion through the enforcement of $\tau = Q_0^{-1}$ for all relevant Q_0 values. There are two immediate advantages of this approach: (i) the search for optimal $\tau^{(p)}$ and $D^{(p)}$ only has to be performed once. Thus, once $\tau^{(p)}$ and $D^{(p)}$ are found, they can be used throughout the earth model even when Q_0 is spatially variable. This statement holds provided that α is constant, which includes the frequency-independent case with $\alpha = 0$. (ii) The explicit appearance of Q_0 facilitates the computation of Fréchet kernels for Q_0 using standard adjoint techniques. The computation of Fréchet kernels for Q_0 and α will be described in Section 3 and illustrated in Section 4.

A numerical example for the case of $N = 3$ relaxation mechanisms and a frequency range from 0.02 to 0.2 Hz is shown in Fig. 1. We determined the parameters $\tau^{(p)}$ and $D^{(p)}$ using Simulated Annealing (Kirkpatrick *et al.* 1983). With $\alpha = 0.3$, $Q(\omega)$ deviates from $Q_{\text{target}}(\omega)$ by less than 3 per cent for values of Q_0 between 50 and 500. While fully sufficient for practical purposes, the accuracy can be improved by using more than three relaxation mechanisms.

2.2 Extension to the elastic case

Following the illustrative example for the scalar wave equation in the previous section, we now transition to the fully elastic 3-D case. We consider both general anisotropy (Section 2.2.1) and the practically most relevant isotropic scenario (Section 2.2.2).

2.2.1 General anisotropy

In analogy to eqs (2) and (3), the momentum conservation and viscoelastic stress–strain relation for generally anisotropic media can be written as

$$\rho \dot{v}_i - \partial_j \sigma_{ij} = f_i \quad (14)$$

and

$$\dot{\sigma}_{ij}(t) = \sum_{k,l=1}^{3} \int_{-\infty}^{\infty} \dot{C}_{ijkl}(t - t') \dot{\epsilon}_{kl}(t') \, \mathrm{d}t' \, , \quad (15)$$

respectively. The stress–strain relation (15) allows different elastic coefficients C_{ijkl} to be subject to different forms of viscoelastic dissipation. These differences may result in anisotropic attenuation that has been predicted for finely layered media (Carcione 1992; Zhu *et al.* 2007) and observed in both laboratory and field experiments (e.g. Tao & King 1990; Bao *et al.* 2012). Anisotropic attenuation in the inner core, with stronger attenuation for waves propagating parallel to the Earth's spin axis, is also well documented (Creager 1992; Song & Helmberger 1993). Generalizing eq. (4) for the time dependence of elastic parameters, we have

$$C_{ijkl}(t) = C^r_{ijkl} \left[1 + \tau_{ijkl} \sum_{p=1}^{N} D^{(p)} \mathrm{e}^{-t/\tau^{(p)}} \right] H(t) \, . \quad (16)$$

Following the developments in Section 2.1.1, we can eliminate the numerically inconvenient convolutional integral in (15) with the help of memory variables: Introducing the time derivative of (16) into the stress–strain relation (15), yields

$$\dot{\sigma}_{ij} = \sum_{k,l=1}^{3} C^r_{ijkl} (1 + \tau_{ijkl} s) \, \dot{\epsilon}_{kl} + \sum_{k,l=1}^{3} C^r_{ijkl} \tau_{ijkl} \sum_{p=1}^{N} M^{(p)}_{kl} \, . \quad (17)$$

The memory variables $M^{(p)}_{kl}$, defined as

$$M^{(p)}_{kl} = -\frac{D^{(p)}}{\tau^{(p)}} \int_{-\infty}^{\infty} \mathrm{e}^{-(t-t')/\tau^{(p)}} H(t - t') \dot{\epsilon}_{kl} \, \mathrm{d}t' \, , \quad (18)$$

satisfy the first-order differential equation

$$\dot{M}_{kl}^{(p)} = -\frac{1}{\tau^{(p)}} M_{kl}^{(p)} - \frac{D^{(p)}}{\tau^{(p)}} \dot{\epsilon}_{kl} \,. \tag{19}$$

Combined, eqs (14)–(16) constitute a complete set of equations that describes the propagation of dissipative waves in anisotropic media.

2.2.2 The isotropic case

Isotropic media described in terms of the bulk modulus κ and the shear modulus μ are the simplest special case of the general viscoelasticity captured in eq. (15). The isotropic elastic tensor is given by

$$C_{ijkl} = \left(\kappa - \frac{2}{3}\mu\right) \delta_{ij}\delta_{kl} + \mu \left(\delta_{ik}\delta_{jl} + \delta_{jk}\delta_{il}\right). \tag{20}$$

Using the fact that the relaxation parameters $\tau^{(p)}$ and $D^{(p)}$ are determined such that the τ_{ijkl} from eq. (16) are equal to the inverses of their corresponding Q_0's, we can write the time-dependent C_{ijkl} as

$$\begin{aligned} C_{ijkl}(t) = {} & \kappa^r \delta_{ij}\delta_{kl} \left[1 + Q_{0\kappa}^{-1} \sum_{p=1}^{N} D^{(p)} \mathrm{e}^{-t/\tau^{(p)}}\right] H(t) \\ & + \mu^r \left(\delta_{ik}\delta_{jl} + \delta_{il}\delta_{jk} - \frac{2}{3}\delta_{ij}\delta_{kl}\right) \\ & \times \left[1 + Q_{0\mu}^{-1} \sum_{p=1}^{N} D^{(p)} \mathrm{e}^{-t/\tau^{(p)}}\right] H(t) \,. \end{aligned} \tag{21}$$

Inserting the time derivative of (21) into the stress–strain relation (15) yields the modified stress–strain relation

$$\begin{aligned} \dot{\sigma}_{ij} = {} & \kappa^r \left[1 + Q_{0\kappa}^{-1} s\right] \dot{\epsilon}_{kk}\delta_{ij} + 2\mu^r \left[1 + Q_{0\mu}^{-1} s\right] \dot{\tilde{\epsilon}}_{ij} \\ & + \kappa^r Q_{0\kappa}^{-1} \sum_{p=1}^{N} M_{kk}^{(p)} \delta_{ij} + 2\mu^r Q_{0\mu}^{-1} \sum_{p=1}^{N} \tilde{M}_{ij}^{(p)} \,. \end{aligned} \tag{22}$$

where ϵ_{kk} and $\tilde{\epsilon}$ denote the trace and the deviator of the strain tensor ϵ_{ij}. Similarly, $M_{kk}^{(p)}$ and $\tilde{M}_{ij}^{(p)}$ are the trace and the deviator of the memory variable tensor $M_{ij}^{(p)}$, defined as in eq. (18). The first two terms in eq. (22) represent a purely elastic stress–strain relation. The last two terms involving the memory variables account for viscoelastic dissipation.

3 SENSITIVITY KERNELS

In Section 2, we established forward problem equations that link viscoelastic parameters to the seismic wavefield. In what follows, we will use this link in order to derive expressions for Fréchet kernels with respect to Q and α. For this, we assume that a measurement, encoded in the measurement functional $\chi(\mathbf{u})$, has been made. Possible measurements include L_1 and L_2 waveform differences (Brossier *et al.* 2009, 2010), cross-correlation traveltimes (Luo & Schuster 1991), generalized seismological data functionals (Gee & Jordan 1992), or various time–frequency misfits (Fichtner *et al.* 2008). Our analysis rests on the adjoint method, described, for instance, by Tarantola (1984), Tromp *et al.* (2005), Fichtner *et al.* (2006a,b) or Chen (2011).

3.1 Adjoint equations and adjoint memory variables

Invoking the adjoint method, the variation $\delta\chi$ of the measurement functional can be written in terms of the forward wavefield $\mathbf{u}$, the forward strain tensor $\boldsymbol{\epsilon}$, the adjoint wavefield $\mathbf{u}^\dagger$, the adjoint strain tensor $\boldsymbol{\epsilon}^\dagger$, the variation in density $\delta\rho$, and the variation of the elastic tensor $\delta\mathbf{C}$:

$$\begin{aligned} \delta\chi = {} & -\int_{-\infty}^{\infty}\int_{V} \delta\rho\, \dot{u}_i^\dagger(t)\dot{u}_i(t)\,\mathrm{d}\mathbf{x}\,\mathrm{d}t \\ & + \int_{-\infty}^{\infty}\int_{V} \left[\int_{-\infty}^{\infty} \epsilon_{ij}^\dagger(t)\,\delta\dot{C}_{ijkl}(t-t')\,\epsilon_{kl}(t')\,\mathrm{d}t'\right] \mathrm{d}\mathbf{x}\,\mathrm{d}t \,. \end{aligned} \tag{23}$$

The adjoint field is governed by the adjoint equations that may be written in velocity–stress formulation, consisting of the momentum conservation equation

$$\rho\dot{v}_i^\dagger - \partial_j\sigma_{ij}^\dagger = f_i^\dagger \tag{24}$$

and the stress–strain relation

$$\dot{\sigma}_{ij}^\dagger = \int_{-\infty}^{\infty} \dot{C}_{ijkl}(t'-t)\dot{\epsilon}_{kl}^\dagger(t')\,\mathrm{d}t' \,. \tag{25}$$

The adjoint source $f_i^\dagger$ is determined by the definition of the measurement, that is by the specific form of χ (see Section 4 for examples). Viscoelastic dissipation in the adjoint stress-strain relation is time-reversed, meaning that current stresses depend on future strains. Since the adjoint equations are, however, solved in reverse time, numerical stability is ensured (Tarantola 1988; Fichtner 2010). Again following the developments in Section 2.1.1, we eliminate the convolutional integral in (25) by defining adjoint memory variables $M_{kl}^{(p)\dagger}$ as

$$M_{kl}^{(p)\dagger} = -\frac{D^{(p)}}{\tau^{(p)}} \int_{-\infty}^{\infty} \mathrm{e}^{-(t'-t)/\tau^{(p)}} H(t'-t)\dot{\epsilon}_{kl}^\dagger\,\mathrm{d}t' \,. \tag{26}$$

Differentiating eq. (26) with respect to time t, it follows that the adjoint memory variables satisfy the first-order differential equation

$$\dot{M}_{kl}^{(p)\dagger} = \frac{1}{\tau^{(p)}} M_{kl}^{(p)\dagger} + \frac{D^{(p)}}{\tau^{(p)}} \dot{\epsilon}_{kl}^\dagger \,. \tag{27}$$

The resulting modified stress–strain relation for the adjoint field is

$$\dot{\sigma}_{ij}^\dagger = C_{ijkl}^r (1 + \tau_{ijkl} s)\,\dot{\epsilon}_{kl}^\dagger + \sum_{k,l=1}^{3} C_{ijkl}^r \tau_{ijkl} \sum_{p=1}^{N} M_{kl}^{(p)\dagger} \,. \tag{28}$$

Equipped with the complete set of adjoint equations, consisting of eqs (23), (27) and (28), we can proceed with the calculation of sensitivity kernels for Q and α. In the interest of a lighter notation, we will consider shear and bulk Q separately, and we transfer the detailed derivation of α kernels to the Appendix.

3.2 Shear Q

Restricting ourselves to an isotropic medium with $C_{ijkl} = (\kappa - \frac{2}{3}\mu)\delta_{ij}\delta_{kl} + \mu\delta_{ik}\delta_{jl} + \mu\delta_{il}\delta_{jk}$ and variations in the shear modulus μ, eq. (23) condenses to

$$\delta\chi = 2\int_{-\infty}^{\infty}\int_{V} \left[\int_{-\infty}^{\infty} \tilde{\epsilon}_{ij}^\dagger(t)\,\delta\dot{\mu}(t-t')\,\mathrm{d}t\right] \tilde{\epsilon}_{ij}(t')\,\mathrm{d}\mathbf{x}\,\mathrm{d}t' \,, \tag{29}$$

where $\tilde{\epsilon}_{ij}$ and $\tilde{\epsilon}^{\dagger}_{ij}$ are the deviatoric parts of ϵ_{ij} and $\epsilon^{\dagger}_{ij}$, respectively. Invoking the chain rule, we can express $\delta\mu$ in (29) in terms of variations in $Q_{0\,\mu}$:

$$\delta\mu = \frac{\partial\mu}{\partial Q_{0\,\mu}}\,\delta Q_{0\,\mu}\,. \tag{30}$$

The partial derivatives $\partial\mu/\partial Q_{0\,\mu}$ follows from the definition of the time-dependent elastic modulus in (4), with the general relaxed modulus C^r set equal to the relaxed shear modulus μ^r:

$$\frac{\partial\mu(t)}{\partial Q_{0\,\mu}} = -\mu^r\, Q_{0\,\mu}^{-2}\left[\sum_{p=1}^{N} D^{(p)}\mathrm{e}^{-t/\tau^{(p)}}\right] H(t)\,. \tag{31}$$

Using (30) and (31), we can reformulate the integral over $\tilde{\epsilon}^{\dagger}_{ij}(t)\delta\dot{\mu}(t-t')$ that appears in eq. (29):

$$\begin{aligned}\int_{-\infty}^{\infty} \tilde{\epsilon}^{\dagger}_{ij}(t)\,\delta\dot{\mu}(t-t')\,\mathrm{d}t &= \int_{-\infty}^{\infty} \dot{\tilde{\epsilon}}^{\dagger}_{ij}(t)\,\delta\mu(t-t')\,\mathrm{d}t \\ &= -\mu^r\, Q_{0\,\mu}^{-2}\sum_{p=1}^{N}\int_{-\infty}^{\infty} D^{(p)}e^{(t-t')/\tau(p)}H(t-t')\,\dot{\tilde{\epsilon}}^{\dagger}_{ij}(t)\,\delta Q_{0\,\mu}\,\mathrm{d}t\,.\end{aligned} \tag{32}$$

Identifying copies of the adjoint memory variables $M^{(p)\,\dagger}_{kl}$, defined in (26), we can condense (32) into

$$\int_{-\infty}^{\infty} \tilde{\epsilon}^{\dagger}_{ij}(t)\,\delta\dot{\mu}(t-t')\,\mathrm{d}t = \mu^r\, Q_{0\,\mu}^{-2}\sum_{p=1}^{N}\tau^{(p)}\tilde{M}^{(p)\,\dagger}_{ij}(t')\,\delta Q_0\,. \tag{33}$$

We can now combine (29) with (33) in order to write $\delta\chi$ in terms of the volumetric Fréchet or sensitivity kernel $K_{Q_{0\,\mu}}$:

$$\delta\chi = \int_V K_{Q_{0\,\mu}}(\mathbf{x})\,\delta\ln Q_{0\,\mu}(\mathbf{x})\,\mathrm{d}\mathbf{x}\,, \tag{34}$$

where $K_{Q_{0\,\mu}}$ can be explicitly computed from the interaction of the forward strain deviator $\tilde{\epsilon}_{ij}$ and the deviator of the adjoint memory variables, $\tilde{M}_{p,ij}$:

$$K_{Q_{0\,\mu}} = 2\mu^r\, Q_{0\,\mu}^{-1}\sum_{p=1}^{N}\tau^{(p)}\int_{-\infty}^{\infty}\tilde{M}^{(p)\,\dagger}_{ij}\tilde{\epsilon}_{ij}\,\mathrm{d}t\,. \tag{35}$$

Eq. (35) reveals that the kernel for $Q_{0\,\mu}$ can be computed in a similar fashion as kernels for elastic parameters, velocity and density; without any additional computational requirements. The adjoint equations are solved in reversed time which automatically yields the adjoint memory variables needed to evaluate the time integrals in (35). For comparison, the sensitivity kernel for the shear modulus μ in a non-dissipative medium is given by (e.g. Tromp *et al.* 2005; Fichtner 2010)

$$K_{\mu} = 2\mu\int_{-\infty}^{\infty}\tilde{\epsilon}^{\dagger}_{ij}\tilde{\epsilon}_{ij}\,\mathrm{d}t\,. \tag{36}$$

Thus, for the computation of the Q kernel $K_{Q_{0\,\mu}}$, the term $Q_{0\,\mu}^{-1}\sum_{p=1}^{N}\tau^{(p)}\tilde{M}^{(p)\,\dagger}_{ij}$, involving the deviator of the adjoint memory variables, simply takes the place of the adjoint strain tensor $\tilde{\epsilon}^{\dagger}_{ij}$ in eq. (36). Following similar steps as above, we show in the Appendix that the Fréchet kernel K_{α} for the exponent α in the power-law frequency dependence of Q_{μ} (eq. 11), is given by

$$K_{\alpha} = -2\mu^r\,\alpha\, Q_{0\,\mu}^{-1}\sum_{p=1}^{N}\frac{\tau^{(p)}}{D^{(p)}}\frac{\partial D^{(p)}}{\partial\alpha}\int_{-\infty}^{\infty}\tilde{M}^{(p)\,\dagger}_{ij}\tilde{\epsilon}_{ij}\,\mathrm{d}t\,. \tag{37}$$

3.3 Bulk Q

Considering only variations in the viscoelastic properties related to the bulk modulus κ, the variation of the elastic tensor C_{ijkl} reduces to $\delta C_{ijkl} = \delta\kappa$. The variation of the misfit or measurement functional χ can then be written in terms of the traces ϵ_{kk} and $\epsilon^{\dagger}_{kk}$ of the forward and adjoint strain tensors:

$$\delta\chi = \int_{-\infty}^{\infty}\int_V\left[\int_{-\infty}^{\infty}\epsilon^{\dagger}_{kk}(t)\,\delta\dot{\mu}(t-t')\,\mathrm{d}t\right]\epsilon_{kk}(t')\,\mathrm{d}\mathbf{x}\,\mathrm{d}t'\,. \tag{38}$$

Following exactly the same steps as in Section 3.2 on shear Q, we can transform (38) into

$$\delta\chi = \int_V K_{Q_{0\,\kappa}}(\mathbf{x})\,\delta\ln Q_{0\,\kappa}(\mathbf{x})\,\mathrm{d}\mathbf{x}\,, \tag{39}$$

with the sensitivity kernel

$$K_{Q_{0\,\kappa}} = \kappa^r\, Q_{0\,\kappa}^{-1}\sum_{p=1}^{N}\tau^{(p)}\int_{-\infty}^{\infty}M^{(p)\,\dagger}_{kk}\epsilon_{kk}\,\mathrm{d}t\,. \tag{40}$$

In eq. (40), $M^{(p)\,\dagger}_{kk}$ denotes the trace of the memory variable tensor $M^{(p)\,\dagger}_{ij}$. Just as the kernel for shear Q in eq. (35), the kernel for bulk Q can be computed from the forward strain and the adjoint memory variables that are a natural by-product of the adjoint solution. Again, for comparison, we note the kernel for the bulk modulus κ in a non-dissipative medium is given by (e.g. Tromp *et al.* 2005; Fichtner 2010)

$$K_{\kappa} = \kappa\int_{-\infty}^{\infty}\epsilon^{\dagger}_{kk}\epsilon_{kk}\,\mathrm{d}t\,. \tag{41}$$

It follows that a simple replacement of $\epsilon^{\dagger}_{kk}$ by $Q_{0\,\kappa}^{-1}\sum_{p=1}^{N}\tau^{(p)}M^{(p)\,\dagger}_{kk}$ in eq. (40) yields Q instead of κ kernels.

In the Appendix, we demonstrate that the Fréchet kernel for the power-law exponent of bulk Q is given by

$$K_{\alpha} = -\kappa^r\,\alpha\, Q_{0\,\kappa}^{-1}\sum_{p=1}^{N}\frac{\tau^{(p)}}{D^{(p)}}\frac{\partial D^{(p)}}{\partial\alpha}\int_{-\infty}^{\infty}M^{(p)\,\dagger}_{kk}\epsilon_{kk}\,\mathrm{d}t\,. \tag{42}$$

4 EXAMPLES

To illustrate the practical implementation of frequency-dependent Q and its effect on seismic waveforms, as well as the computation of Q and α kernels, we present various examples from global- and regional-scale wave propagation.

4.1 Global wave propagation

In order to model global seismic wave propagation in a broad frequency range, while keeping the computational requirements at a manageable level, we limit ourselves to the radially symmetric

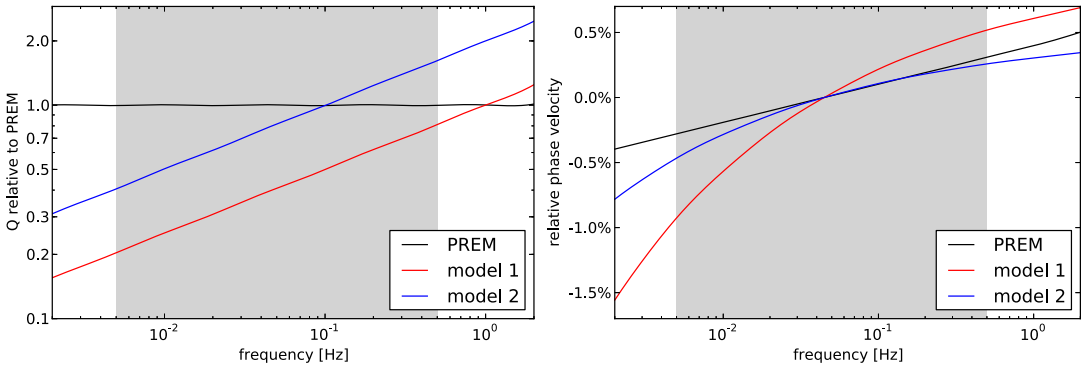

Figure 2. Left-hand panel: Q as a function of frequency as approximated with linear solids and used in the global example shown in Fig. 3. The original frequency-independent Q of PREM (Dziewoński & Anderson 1981) is shown in black. Two frequency-dependent versions of Q are shown in red (reference frequency 1 Hz) and blue (reference frequency 0.1 Hz). Right-hand panel: Phase velocity dispersion relative to the phase velocity of PREM for $Q_0 = 1000$ and the Q models shown to the left-hand side. Velocities are fixed to PREM velocities at the central period of the simulation (22 s) causing the red model to produce smaller traveltimes at short periods. The frequency range used in the example is indicated by grey shading.

earth model PREM (Dziewoński & Anderson 1981). Being a special case of an axisymmetric medium, the equations of motion for PREM can be reduced to a system of PDE's in two space variables, and solved efficiently by the time-domain spectral-element code AxiSEM (Nissen-Meyer *et al.* 2007, 2014; van Driel & Nissen-Meyer 2014b).

We consider three different Q models, summarized in the left-hand panel of Fig. 2. The original, frequency-independent Q of PREM (black curve), a frequency-dependent Q with $\alpha = 0.3$ and reference frequency 1 Hz (red curve), and a frequency-dependent Q with $\alpha = 0.3$ and reference frequency 0.1 Hz (blue curve). The phase velocities are matched to the phase velocities of PREM at the central period of the numerical simulation, which is 22 s. The resulting phase velocity dispersion curves are shown in the right-hand panel of Fig. 2.

The frequency dependence of Q and the different choice in reference frequency lead to notable differences in synthetic seismograms, a small collection of which is presented in Fig. 3 for a period band ranging from 2 to 200 s. The example illustrates that the frequency-dependence of Q is generally not a small effect because realistic values of α between 0.2 and 0.4 (e.g. Karato 2008) can lead to substantial modification of Q away from the reference frequency.

4.2 Regional-scale wave propagation

In our next example, we consider wave propagation at regional scales, that is over distances of few hundred kilometres. Our computational domain, shown in the upper right-hand panel of Fig. 4, is centred on Turkey. We locate the earthquake in eastern Turkey and choose an explosion as source mechanism in order to exclude radiation pattern effects on the sensitivity kernels computed in the following sections. As earth model we again use PREM (Dziewoński & Anderson 1981), modified such that Q_μ and Q_κ are frequency dependent as shown in Fig. 1. For the simulation of 3-D seismic wave propagation, we use the spectral-element solver SES3D, described in Fichtner & Igel (2008) and Fichtner *et al.* (2009).

A comparison of synthetic seismograms with and without attenuation is shown in Fig. 4 for station ADVT, located in western Turkey at an epicentral distance of 9°. As a result of the short epicentral distance and the short dominant period of 8 s, the wavefield mostly senses crustal and uppermost mantle structure where Q_μ and Q_κ in PREM range around 600 and 58 000, respectively. It follows that the effects on phase and amplitude are small, but noticeable. The amplitudes of both body and surface waves are reduced by around 5 per cent. The time shifts induced by the presence of viscoelastic attenuation range around 1 s.

For the calculation of Fréchet kernels we limit ourselves to two types of measurements: (1) Relative L_2 amplitude differences are defined as

$$\chi = A = \frac{\int u^2 \, \mathrm{d}t - \int u_0^2 \, \mathrm{d}t}{\int u_0^2 \, \mathrm{d}t} \,, \tag{43}$$

with u and u_0 denoting synthetic and observed seismograms, respectively. For our examples, we restrict ourselves to the vertical components, that is $u = u_z$. (2) Correlation traveltime shifts are defined as the time T where the correlation between observed and synthetic waveforms reaches its maximum (e.g Luo & Schuster 1991; Dahlen *et al.* 2000):

$$\chi = T = \arg\max \int u(\tau)\, u_0(t+\tau) \, \mathrm{d}\tau \,. \tag{44}$$

The adjoint sources $\mathbf{f}^\dagger$ for these measurements, that is the right-hand sides of the adjoint eq. (24), are given by

$$\mathbf{f}_A^\dagger(t) = \frac{2u(t)}{\int u^2 \, \mathrm{d}t} \, \mathbf{e}_z \,, \tag{45}$$

and

$$\mathbf{f}_T^\dagger(t) = -\frac{\dot{u}(t)}{\int \dot{u}^2 \, \mathrm{d}t} \, \mathbf{e}_z \,, \tag{46}$$

respectively (e.g. Luo & Schuster 1991; Fichtner 2010). Equipped with eqs (45) and (46), we can solve the adjoint equations that provide the adjoint memory variables needed to compute Fréchet kernels for viscoelastic parameters, according to eqs (35) and (40).

4.2.1 *Fréchet kernels for Q at the reference frequency*

Fig. 5 displays horizontal slices through Fréchet kernels for $Q_{0\mu}$, that is the shear Q at the reference circular frequency ω_0. Kernels are computed based on eq. (35) and for measurements performed in three different time windows. While the time window from 246 to 333 s mostly contains higher-mode Rayleigh waves, the time window from 362 to 400 s is dominated by the fundamental-mode Rayleigh wave. Acknowledging that more elaborate measurements—based for instance on multitapers or various time-frequency transforms (e.g. Laske & Masters 1996; Zhou *et al.* 2004; Fichtner *et al.* 2008)—are possible, we do not apply additional

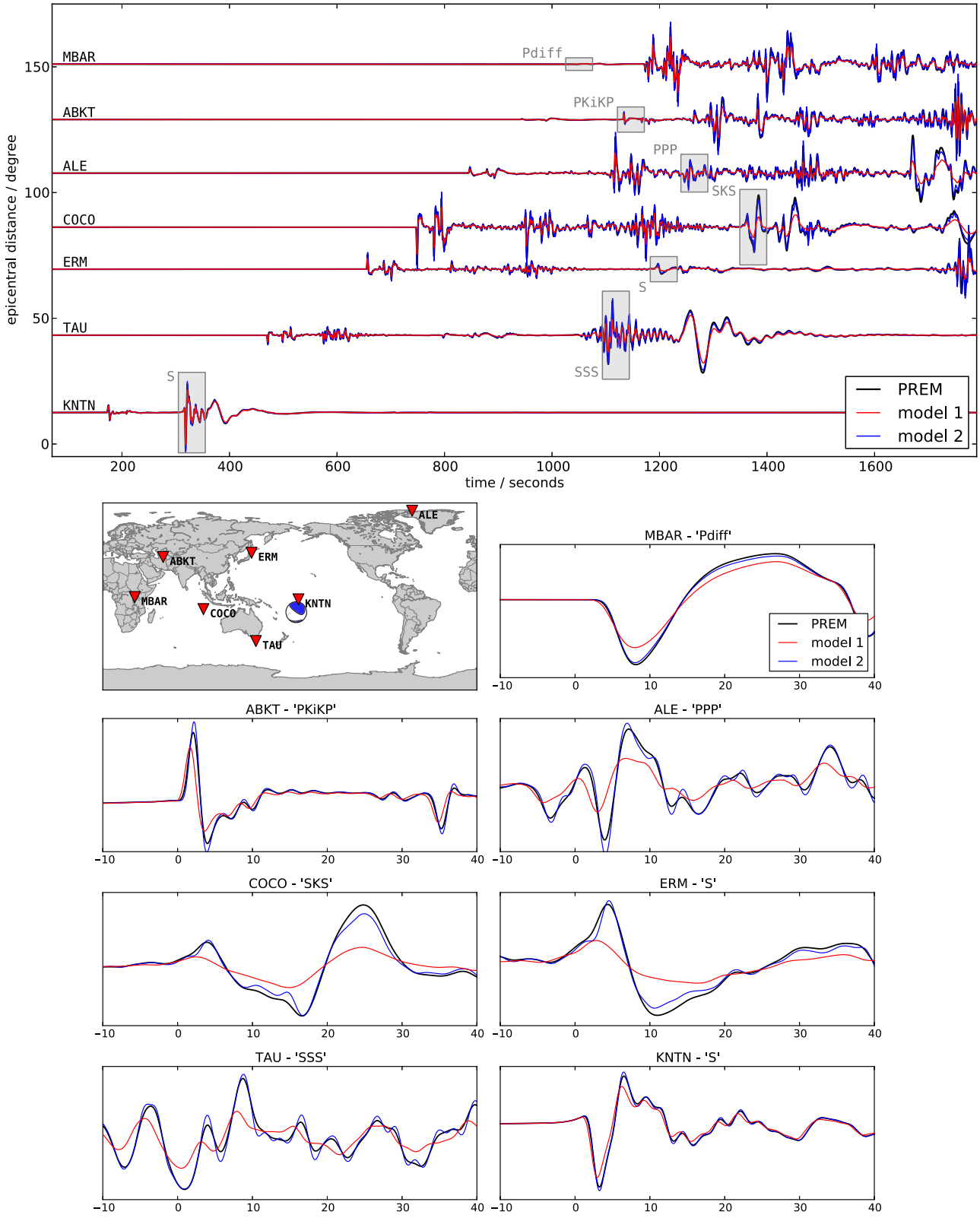

Figure 3. Comparison of vertical-component displacement seismograms (bandpass filtered between 2 and 200 s period) for a moment magnitude $M_w = 5.0$ event in 126 km depth under the Tonga islands, computed with AxiSEM in the anisotropic PREM model without ocean with the three different attenuation models shown in Fig. 2. The traces are plotted for the GSN stations indicated in the map. The zoom windows are indicated with red rectangles in the record section and the timescale is relative to the ray-theoretical arrival.

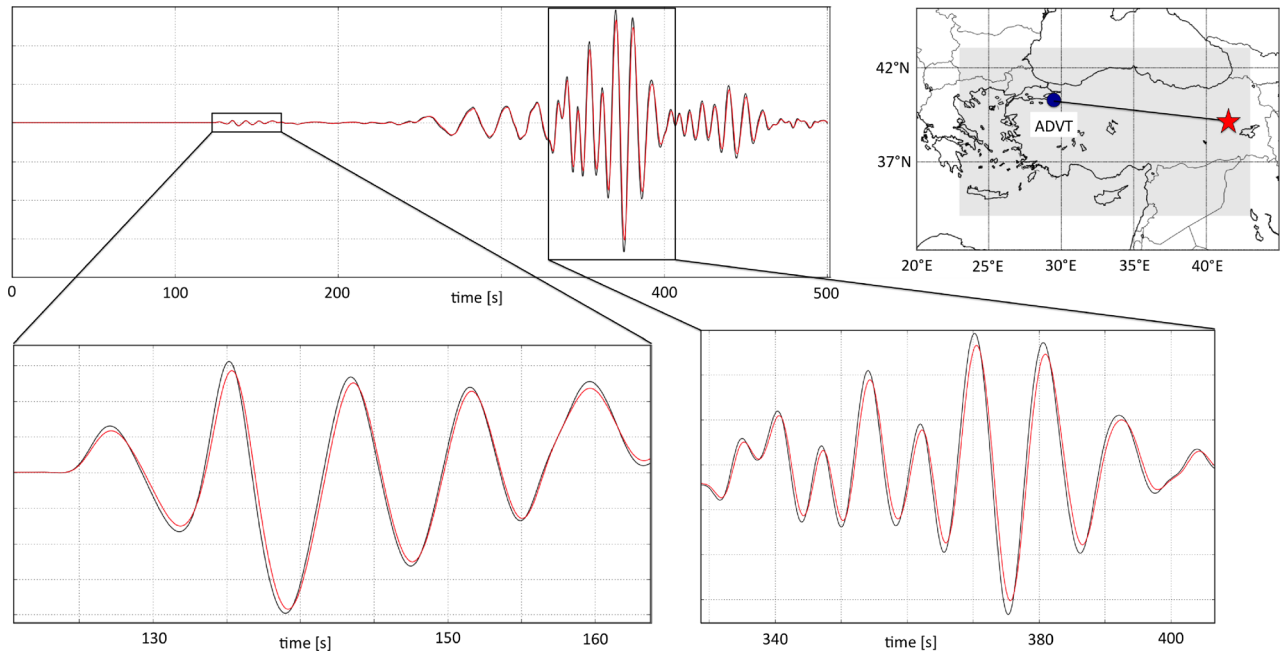

Figure 4. Comparison of vertical-component synthetic seismograms without (black) and with (red) viscoelastic dissipation for a dominant period of 8 s. The source–receiver configuration is shown to the right-hand side, with the computational domain shaded in light grey. As earth model, we use the spherically symmetric PREM (Dziewoński & Anderson 1981) with a frequency-dependent Q constructed as in Fig. 1. The zoom into the P wave and surface wave trains (lower left- and lower right-hand side, respectively), reveals time shifts of around 1 s and amplitude variations on the order of 5 per cent.

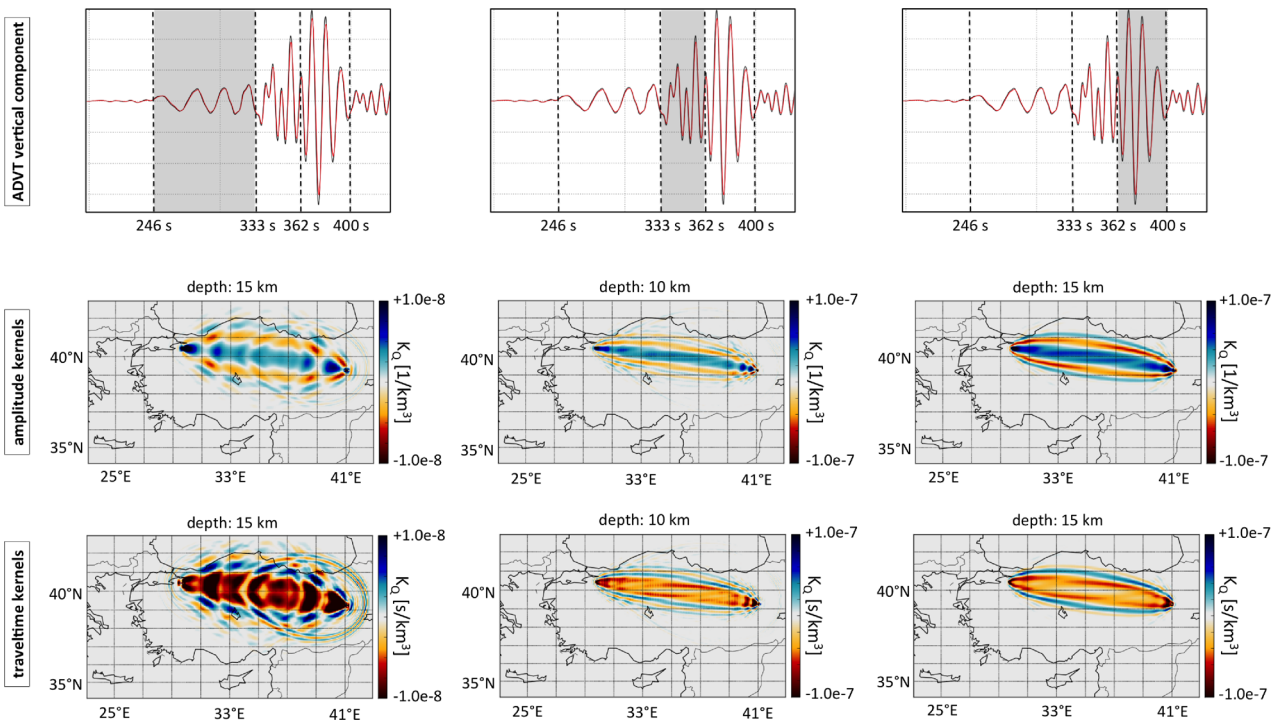

Figure 5. Horizontal slices through Fréchet kernels for relative perturbations in $Q_{0\,\mu}$ for measurements in different time windows on the vertical-component velocity seismogram from station ADVT (see Fig. 4). The time windows are indicated in the top row by grey shading. Kernels for amplitude and traveltime measurements are shown in the second and third row, respectively. All kernels are plotted at the depth where they attain their largest values. Note the different colour scales.

filters or time windows in order to keep the examples illustrative and repeatable. Kernels for amplitude and traveltime measurements are shown in the second and third rows of Fig. 5, respectively. All kernels are plotted at the depth where they attain their maximum values.

Being a composite of various higher modes, the time window from 246 to 333 s yields Fréchet kernels that deviate from the simple cigar shape produced by the fundamental-mode Rayleigh wave in the 362–400 time window. The comparatively high frequencies in the time window from 333 to 362 s lead to a thinner Fresnel

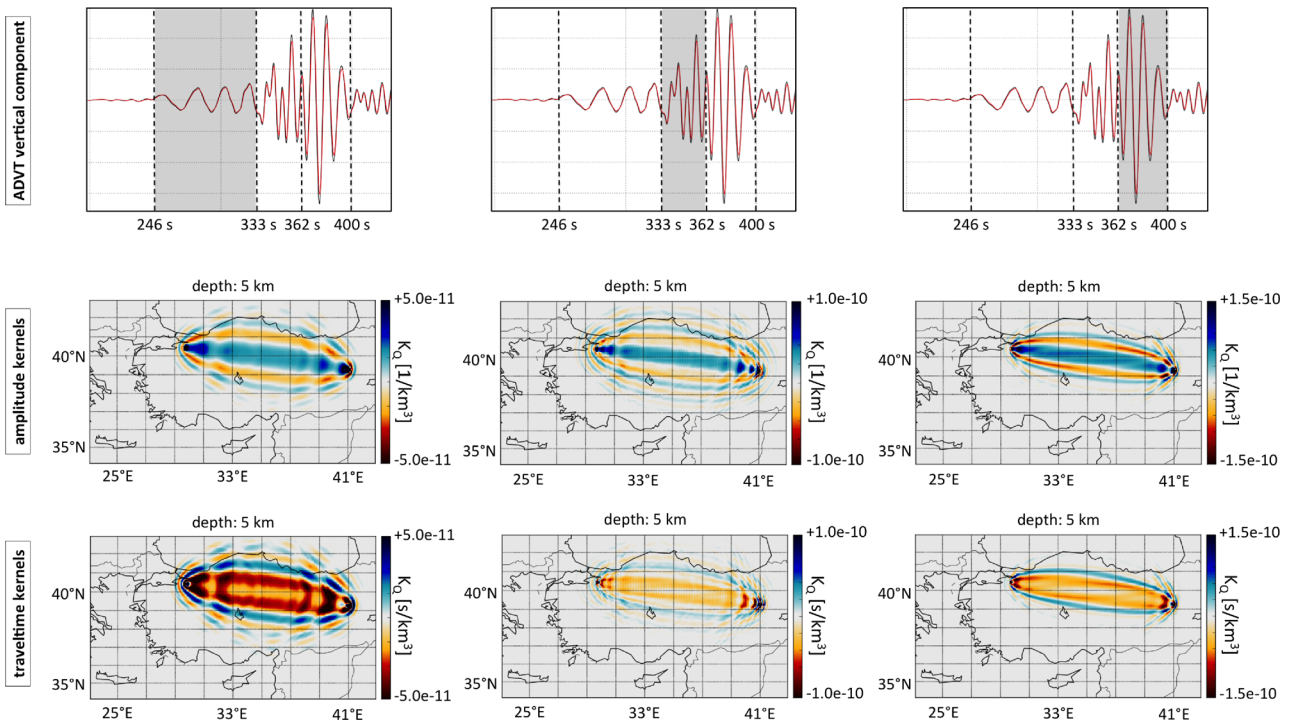

Figure 6. The same as Fig. 5 but for relative perturbations in the bulk quality factor $Q_{0\kappa}$.

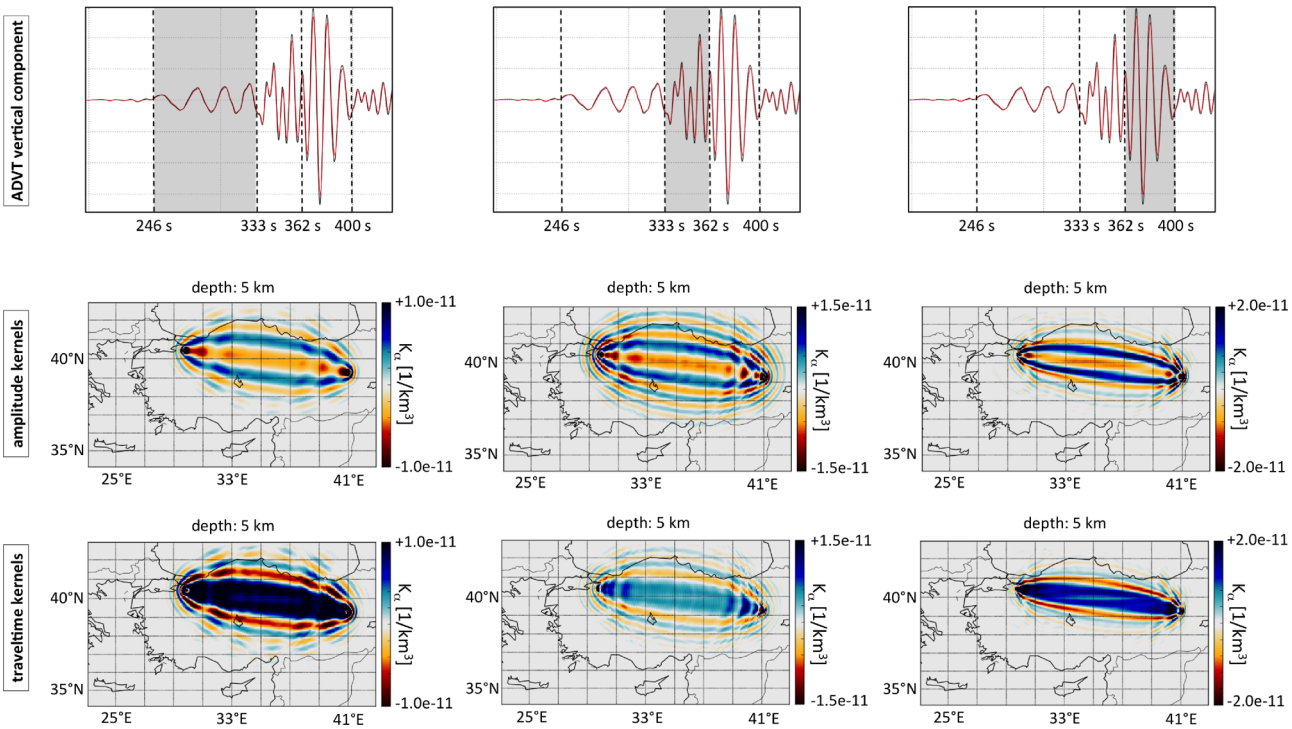

Figure 7. The same as Fig. 5 but for relative perturbations in the exponent α of the shear quality factor Q_μ.

zone than for the other time windows where the dominant frequencies are lower. Generally, amplitude and traveltime measurements have similarly strong sensitivity to relative perturbations in $Q_{0\mu}$, as previously noted, for instance, by Zhou (2009).

Fréchet kernels for $Q_{0\kappa}$, that is bulk Q at the reference frequency, can be computed using eq. (40). Kernels for the same measurement windows and measurements as in Fig. 5 are shown in Fig. 6. As expected for surface waves with little sensitivity to the bulk modulus, sensitivities for bulk Q are several orders of magnitude smaller than for shear Q. The overall geometrical pattern, however, remains unchanged.

4.2.2 Fréchet kernels for the power-law exponent α

The computation of Fréchet kernels for α, that is the power-law exponent in the frequency dependence of Q, requires knowledge

of the partial derivatives $\partial D^{(p)}/\partial\alpha$ (see eqs 37 and 42). Since the weights $D^{(p)}$ are computed by numerical optimization as outlined in Section 2.1.2, their partial derivatives are not explicitly available. They can, however, be approximated by computing weights $D^{(p)}(\alpha+\delta\alpha)$ for a slightly perturbed power-law exponent α:

$$\frac{\partial D^{(p)}}{\partial\alpha} \approx \frac{D^{(p)}(\alpha+\delta\alpha) - D^{(p)}(\alpha)}{\delta\alpha}. \tag{47}$$

For our example with three relaxation mechanisms, the finite-difference approximation (47) yields the values $\partial D^{(1)}/\partial\alpha = -3.06$, $\partial D^{(2)}/\partial\alpha = -1.54$ and $\partial D^{(3)}/\partial\alpha = 2.56$ for shear Q.

Fréchet kernels for fractional perturbations in shear α, displayed in Fig. 7 for the previously used time windows and measurements, are orders of magnitude smaller than kernels for fractional perturbations in shear Q. While more targeted measurements are possible (e.g. Cheng & Kennett 2002; Lekić *et al.* 2009; Kennett & Abdullah 2011), this result still reflects that the frequency-dependence of Q in the Earth is difficult to constrain.

5 DISCUSSION AND CONCLUSIONS

We presented a novel method for the modelling of frequency-dependent and frequency-independent Q in time-domain numerical wave propagation. In contrast to previous approaches (e.g. Emmerich & Korn 1987; Carcione *et al.* 1988a,b; Blanch *et al.* 1995), Q as a function of position in the Earth is introduced explicitly into the equations of motion.

A key element of our method is the determination of only one set of relaxation parameters $\tau^{(p)}$ and $D^{(p)}$ from eq. (4) that is valid for the full range of Q_0 values in the earth model. This is different from more classical approaches where a set of relaxation parameters is determined individually for each Q_0 value (e.g. Emmerich & Korn 1987; Blanch *et al.* 1995; van Driel & Nissen-Meyer 2014a). A direct consequence of working with one universal set of relaxation parameters are larger discrepancies between the target Q model and the actual numerical Q model. For most practical purposes, however, these errors are hardly relevant. Using, for instance, $N = 3$ relaxation mechanisms for frequencies between 0.02 and 0.2 Hz, and Q_0 between 50 and 500, the relative errors between the target Q and the numerical Q shown in Fig. 1 are below 3 per cent. This error is well below lateral variations of shear Q in global models that are on the order of $\pm$100 per cent (e.g. Romanowicz 1995; Selby & Woodhouse 2002; Warren & Shearer 2002; Gung & Romanowicz 2004; Dalton *et al.* 2008). Differences between 1-D Q models typically range between 10 and 100 per cent (e.g. Dziewoński & Anderson 1981; Widmer *et al.* 1991; Durek & Ekström 1996; Resovsky *et al.* 2005; Trampert & Fichtner 2013).

The most relevant tuning parameters in our approach are the number and values of the target $Q_0^{(k)}$, as well as the number of relaxation parameters. While one should ideally give a generally valid recipe for the perfect distribution of the target $Q_0^{(k)}$, we think that carefully conducted numerical experiments with different choices for $Q_0^{(k)}$ are more likely to provide good results for specific applications with their specific requirements. The same holds for the number of relaxation mechanisms. The approximation can be improved through the incorporation of additional relaxation mechanisms, though at the expense of increase computational costs.

The α kernels derived in the Appendix and computed in Section 4.2.2 for example measurements, in principle provide a tool that enables inversions for the frequency-dependence of Q as a function of position. Since Q itself tends to be poorly resolved (e.g. Resovsky *et al.* 2005), a good spatial resolution of α, that is comparable to the spatial resolution of seismic velocities, seems unlikely. Model basis functions for α will thus need to have a broader spatial extent, or even be constant for the whole Earth—depending on the resolving power of a specific data set. In our description of Q, we so far assumed a constant α throughout the Earth. In the case of spatially variable α, this aspect would need to be relaxed, and position dependent weight factors $D^{(p)}$ would need to be determined.

The most important advantage of our approach lies in the computationally efficient calculation of Fréchet kernels that does not require additional computational costs, compared to the calculation of Fréchet kernels for elastic properties. Fréchet kernels for anelastic properties can generally be expressed in terms of the forward strain field and the adjoint memory variables that are a by-product of any adjoint calculation in a viscoelastic medium.

ACKNOWLEDGEMENTS

The authors would like to thank the editor Andrea Morelli, as well as Ebru Bozdag and Yann Capdeville for their thoughtful and constructive reviews. We gratefully acknowledge support from the European Commission (Marie Curie Actions, ITN QUEST, www.quest-itn.org) and the Netherlands Organisation for Scientific Research (VIDI grant 864.11.008). Data processing was partly done using the *ObsPy* toolkit (Beyreuther *et al.* 2010; Megies *et al.* 2011). Computations where performed at the ETH central HPC cluster (Brutus), the Swiss National Supercomputing Center (CHRONOS project ch1) and the UK National Supercomputing Service (HECToR/Archer).

REFERENCES

Aki, K. & Richards, P., 2002. *Quantitative Seismology,* University Science Books.

Anderson, D.L. & Minster, J.B., 1979. The frequency dependence of Q in the Earth and implications from mantle rheology and Chandler wobble, *Geophys. J. R. astr. Soc.,* **58,** 431–440.

Bao, X., Sandvol, E., Chen, Y.J., Ni, J., Hearn, T. & Shen, Y., 2012. Azimuthal anisotropy of Lg attenuation in eastern Tibetan Plateau, *J. geophys. Res.,* **117,** doi:10.1029/2012Jb009255.

Beyreuther, M., Barsch, R., Krischer, L. & Wassermann, J., 2010. ObsPy: A Python toolbox for seismology, *Seismol. Res. Lett.,* **81,** 47–58.

Blanch, J.O., Robertsson, J.O.A. & Symes, W.W., 1995. Modelling of a constant Q: methodology and algorithm for an efficient and optimally inexpensive viscoelastic technique, *Geophysics,* **60,** 176–184.

Bozdağ, E., Trampert, J. & Tromp, J., 2011. Misfit functions for full waveform inversion based on instantaneous phase and envelope measurements, *Geophys. J. Int.,* **185,** 845–870.

Brossier, R., Operto, S. & Virieux, J., 2009. Robust elastic frequency-domain full waveform inversion using the l_1 norm, *Geophys. Res. Lett.,* **36,** L20310, doi:10.1029/2009GL039458.

Brossier, R., Operto, S. & Virieux, J., 2010. Which data residual norm for robust elastic frequency-domain full waveform inversion?, *Geophysics,* **75,** R37–R46.

Carcione, J., 1992. Anisotropic Q and velocity dispersion of finely layered media, *Geophys. Prospect.,* **40,** 761–783.

Carcione, J.M., Kosloff, D. & Kosloff, R., 1988. Wave propagation simulation in a linear viscoelastic medium, *Geophys. J.,* **95,** 597–611.

Chen, P., 2011. Full-wave seismic data assimilation: theoretical background and recent advances, *Geophys. J. Int.,* **168,** 1527–1552.

Chen, P., Zhao, L. & Jordan, T.H., 2007. Full 3D tomography for the crustal structure of the Los Angeles region., *Bull. seism. Soc. Am.,* **97,** 1094–1120.

Cheng, H.-X. & Kennett, B.L.N., 2002. Frequency dependence of seismic wave attenuation in the upper mantle beneath the australian region, *Geophys. J. Int.,* **150**(1), 45–57.

Creager, K.C., 1992. Anisotropy of the inner core from differential travel times of the phases PKP and PKIKP, *Nature,* **356,** 309–314.

Dahlen, F.A. & Tromp, J., 1998. *Theoretical Global Seismology,* Princeton Univ. Press.

Dahlen, F.A., Hung, S.-H. & Nolet, G., 2000. Fréchet kernels for finite-frequency traveltimes—I. Theory, *Geophys. J. Int.,* **141,** 157–174.

Dalton, C.A., Ekström, G. & Dziewonski, A.M., 2008. The global attenuation structure of the upper mantle, *J. geophys. Res.,* **113,** doi:10.1029/2007JB005429.

Dumbser, M., Käser, M. & de la Puente, J., 2007. Arbitrary high order finite volume schemes for seismic wave propagation on unstructured meshes in 2D and 3D, *Geophys. J. Int.,* **171,** 665–694.

Durek, J.J. & Ekström, G., 1996. A radial model of anelasticity consistent with long-period surface wave attenuation, *Bull. seism. Soc. Am.,* **86,** 144–158.

Dziewoński, A.M. & Anderson, D.L., 1981. Preliminary reference Earth model, *Phys. Earth planet. Inter.,* **25,** 297–356.

Emmerich, H. & Korn, M., 1987. Incorporation of attenuation into time-domain computations of seismic wave fields, *Geophysics,* **52,** 1252–1264.

Fichtner, A., 2010. *Full Seismic Waveform Modelling and Inversion,* Springer.

Fichtner, A. & Igel, H., 2008. Efficient numerical surface wave propagation through the optimization of discrete crustal models—a technique based on non-linear dispersion curve matching (DCM), *Geophys. J. Int.,* **173,** 519–533.

Fichtner, A., Bunge, H.-P. & Igel, H., 2006a. The adjoint method in seismology—I. Theory, *Phys. Earth planet. Inter,* **157,** 86–104.

Fichtner, A., Bunge, H.-P. & Igel, H., 2006b. The adjoint method in seismology—II. Applications: traveltimes and sensitivity functionals, *Phys. Earth planet. Inter.,* **157,** 105–123.

Fichtner, A., Kennett, B.L.N., Igel, H. & Bunge, H.-P., 2008. Theoretical background for continental- and global-scale full-waveform inversion in the time-frequency domain, *Geophys. J. Int.,* **175,** 665–685.

Fichtner, A., Kennett, B.L.N., Igel, H. & Bunge, H.-P., 2009. Full seismic waveform tomography for upper-mantle structure in the Australasian region using adjoint methods, *Geophys. J. Int.,* **179,** 1703–1725.

Flanagan, M.P. & Wiens, D.A., 1998. Attenuation of broadband P and S waves in Tonga, *Pure. appl. Geophys.,* **153,** 345–375.

Gee, L.S. & Jordan, T.H., 1992. Generalized seismological data functionals, *Geophys. J. Int.,* **111,** 363–390.

Goetze, C., 1971. High temperature rheology of Westerly granite, *J. geophys. Res.,* **76,** 1223–1230.

Goetze, C. & Brace, W.F., 1972. Laboratory observations of high-temperature rheology of rocks, *Tectonophys.,* **13,** 583–600.

Gueguen, Y., Darot, M., Mazot, P. & Woirgard, J., 1989. Q^{-1} of forsterite single crystals, *Phys. Earth planet. Int.,* **55,** 254–258.

Gung, Y.C. & Romanowicz, B., 2004. Q tomography of the upper mantle using three component long period waveforms, *Geophys. J. Int.,* **157,** 813–830.

Igel, H., Mora, P. & Riollet, B., 1995. Anisotropic wave propagation through FD grids, *Geophysics,* **60,** 1203–1216.

Jackson, I., 2000. Laboratory measurements of seismic wave dispersion and attenuation: recent progress, in *Earth's Deep Interior,* pp. 265–289, eds Karato, S.-I., Forte, A.M., Liebermann, R.C., Masters, G. & Stixrude, L., American Geophysical Union.

Jackson, I., 2007. Physical origins of anelasticity and attenuation in rock, in *Treatise on Geophysics,* pp. 493–525, ed. Schubert, G., Elsevier.

Karato, S.-I., 2008. *Deformation of Earth Materials,* Cambridge Univ. Press.

Karato, S.-I. & Spetzler, H.A., 1990. Defect microdynamics in minerals and solid state mechanisms of seismic wave attenuation and velocity dispersion in the mantle, *Rev. Geophys.,* **28,** 399–421.

Kennett, B.L.N., 2001. *The Seismic Wavefield I.—Introduction and Theoretical Development,* Cambridge Univ. Press.

Kennett, B.L.N. & Abdullah, A., 2011. Seismic wave attenuation beneath the Australasian region, *Aust. J. Earth Sci.,* **58,** 285–295.

Kirkpatrick, S., Gelatt, C.D. & Vecchi, M.P., 1983. Optimization by simulated annealing, *Science,* **220,** 671–680.

Komatitsch, D. & Tromp, J., 1999. Introduction to the spectral element method for three-dimensional seismic wave propagation, *Geophys. J. Int.,* **139,** 806–822.

Laske, G. & Masters, G., 1996. Constraints on global phase velocity maps from long-period polarization data, *J. geophys. Res.,* **101,** 16 059–16 075.

Lekić, V., Matas, J., Panning, M. & Romanowicz, B., 2009. Measurement and implications of frequency dependence of attenuation, *Earth planet. sci. Lett.,* **282,** 285–293.

Liu, H.-P., Anderson, D.L. & Kanamori, H., 1976. Velocity dispersion due to anelasticity: implications for seismology and mantle composition, *Geophys. J. R. astr. Soc.,* **47,** 41–58.

Luo, Y. & Schuster, G.T., 1991. Wave-equation traveltime inversion, *Geophysics,* **56,** 645–653.

Megies, T., Beyreuther, M., Barsch, R., Krischer, L. & Wassermann, J., 2011. Obspy—what can it do for data centers and observatories?, *Ann. Geophys.,* **54,** 47–58.

Moczo, P. & Kristek, J., 2005. On the rheological models for time-domain methods of seismic wave propagation, *Geophys. Res. Lett.,* **32,** doi:10.1029/2004GL021598.

Moczo, P., Kristek, J., Vavrycuk, V., Archuleta, R. & Halada, L., 2002. 3D heterogeneous staggered-grid finite-difference modeling of seismic motion with volume harmonic and arithmetic averaging of elastic moduli, *Bull. seism. Soc. Am.,* **92,** 3042–3066.

Nissen-Meyer, T., Fournier, A. & Dahlen, F.A., 2007. A two-dimensional spectral-element method for computing spherical-Earth seismograms—I. Moment-tensor source, *Geophys. J. Int.,* **168,** 1067–1092.

Nissen-Meyer, T., van Driel, M., Stähler, S., Hosseini, K., Hempel, S., Auer, L. & Fournier, A., 2014. AxiSEM: broadband 3-D seismic wavefields in axisymmetric media, *Solid Earth Discuss.,* **6,** 265–319.

Resovsky, J., Trampert, J. & van der Hilst, R.D., 2005. Error bars for the global seismic Q profile, *Earth planet. Sci. Lett.,* **230,** 413–423.

Robertsson, J.O.A., Blanch, J.O. & Symes, W.W., 1994. Viscoelastic finite-difference modelling, *Geophysics,* **59,** 1444–1456.

Romanowicz, B., 1995. A global tomographic model of shear attenuation in the upper mantle, *J. geophys. Res.,* **100,** 12 375–12 394.

Romanowicz, B. & Mitchell, B.J., 2007. Deep Earth structure—Q of the Earth from crust to core, in *Treatise on Geophysics,* pp. 731–774, Schubert, G., ed., Elsevier.

Selby, N.D. & Woodhouse, J.H., 2002. The Q structure of the upper mantle: constraints from Rayleigh wave amplitudes, *J. geophys. Res.,* **107,** doi:10.1029/2001JB000257.

Sipkin, S. & Jordan, T.H., 1979. Frequency-dependence of QScS, *Bull. seism. Soc. Am.,* **69,** 1055–1079.

Song, X.D. & Helmberger, D., 1993. Anisotropy of the Earth's inner core, *Geophys. Res. Lett.,* **20,** 285–288.

Tao, G. & King, M.S., 1990. Shear-wave velocity and Q anisotropy in rocks: a laboratory study, *Int. J. Rock Mech. Min. Sci. Geomech. Abstr.,* **27,** 353–361.

Tape, C., Liu, Q., Maggi, A. & Tromp, J., 2010. Seismic tomography of the southern California crust based upon spectral-element and adjoint methods, *Geophys. J. Int.,* **180,** 433–462.

Tarantola, A., 1984. Inversion of seismic reflection data in the acoustic approximation, *Geophysics,* **49,** 1259–1266.

Tarantola, A., 1988. Theoretical background for the inversion of seismic waveforms, including elasticity and attenuation, *Pure appl. Geophys.,* **128,** 365–399.

Trampert, J. & Fichtner, A., 2013. Global imaging of the Earth's deep interior: seismic constraints on (an)isotropy, density and attenuation, in *Physics and Chemistry of the Deep Earth,* pp. 324–350, ed. Karato, S., Wiley-Blackwell.

Tromp, J., Tape, C. & Liu, Q., 2005. Seismic tomography, adjoint methods, time reversal and banana-doughnut kernels, *Geophys. J. Int.,* **160,** 195–216.

van Driel, M. & Nissen-Meyer, T., 2014a. Optimized visco-elastic wave propagation for weakly dissipative media, *Geophys. J. Int.,* in press.

van Driel, M. & Nissen-Meyer, T., 2014b. Seismic wave propagation in fully anisotropic axisymmetric media, *Geophys. J. Int.,* in press.

Warren, L.M. & Shearer, P.M., 2002. Mapping lateral variations in upper mantle attenuation by stacking P and PP spectra, *J. geophys. Res.,* **107,** doi:10.1029/2001JB001195.

Widmer, R., Masters, G. & Gilbert, F., 1991. Spherically symmetric attenuation within the Earth from normal mode data, *Geophys. J. Int.,* **104,** 541–553.

Zhou, Y., 2009. Surface-wave sensitivity to 3-D anelasticity, *Geophys. J. Int.,* **178,** 1403–1410.

Zhou, Y., Dahlen, F.A. & Nolet, G., 2004. Three-dimensional sensitivity kernels for surface wave observables, *Geophys. J. Int.,* **158,** 142–168.

Zhu, Y., Tsvankin, I. & Vasconcelos, I., 2007. Effective attenuation anisotropy of thin-layered media, *Geophysics,* **72,** D93–D106.

Zhu, H., Bozdağ, E., Duffy, T.S. & Tromp, J., 2013. Seismic attenuation beneath Europe and the North Atlantic: implications for water in the mantle, *Earth planet. Sci. Lett.,* **381,** 1–11.

APPENDIX A: COMPUTING α-KERNELS

In this Appendix, we provide a detailed derivation of the Fréchet kernels for the exponent α in the power-law frequency dependence of Q, as defined in eq. (11). For this we first note that for $Q_0 \gg 1$, eq. (13) can be transformed to

$$\sum_{p=1}^{N} \frac{D_p \omega \tau^{(p)}}{1+\omega^2 \tau^{(p)\,2}} \approx \left(\frac{\omega_0}{\omega}\right)^{\alpha} . \tag{A1}$$

Keeping the relaxation times for a specific target frequency range fixed, eq. (A1) implies that the vector of weights $\mathbf{D} = (D^{(1)}, \ldots, D^{(N)})^T$ only depends on α and not on Q_0, that is $\mathbf{D} = \mathbf{D}(\alpha)$. Equipped with this result, we now proceed with the calculation of α kernels. In the interest of a lighter notation, we again consider shear and bulk attenuation separately.

A1 Shear attenuation

In isotropic media with $C_{ijkl} = (\kappa - \frac{2}{3}\mu)\delta_{ij}\delta_{kl} + \mu\delta_{ik}\delta_{jl} + \mu\delta_{il}\delta_{jk}$ and variations in the shear modulus μ, the variation of the measurement functional (eq. 23) takes the form

$$\delta\chi = 2 \int_{-\infty}^{\infty} \int_{V} \left[\int_{-\infty}^{\infty} \tilde{\epsilon}^{\dagger}_{ij}(t)\, \delta\dot{\mu}(t-t')\, \mathrm{d}t \right] \tilde{\epsilon}_{ij}(t')\, \mathrm{d}\mathbf{x}\, \mathrm{d}t' , \tag{A2}$$

where $\tilde{\epsilon}_{ij}$ and $\tilde{\epsilon}^{\dagger}_{ij}$ are the deviatoric parts of ϵ_{ij} and $\epsilon^{\dagger}_{ij}$, respectively. In the next step, we express $\delta\mu$ in (29) in terms of variations in α. For this, we invoke the chain rule and the previously noted fact that the weights D_p only depend on α (eq. A1):

$$\delta\mu = \sum_{p=1}^{N} \frac{\partial\mu}{\partial D^{(p)}} \frac{\partial D^{(p)}}{\partial\alpha}\, \delta\alpha . \tag{A3}$$

The partial derivatives $\partial\mu/\partial D_p$ follow from the definition of the time-dependent elastic modulus in (4), with the general relaxed modulus C^r set equal to the relaxed shear modulus μ^r:

$$\frac{\partial\mu(t)}{\partial D^{(p)}} = \mu^r\, Q_{0\,\mu}^{-1} e^{-t/\tau^{(p)}} H(t) . \tag{A4}$$

Using (A3) and (A4), we can reformulate the integral over $\tilde{\epsilon}^{\dagger}_{ij}(t)\delta\dot{\mu}(t-t')$ that appears in eq. (A2):

$$\begin{aligned} \int_{-\infty}^{\infty} \tilde{\epsilon}^{\dagger}_{ij}(t)\, \delta\dot{\mu}(t-t')\, \mathrm{d}t &= \int_{-\infty}^{\infty} \dot{\tilde{\epsilon}}^{\dagger}_{ij}(t)\, \delta\mu(t-t')\, \mathrm{d}t \\ &= \mu^r\, Q_{0\,\mu}^{-1} \sum_{p=1}^{N} \int_{-\infty}^{\infty} \frac{\partial D^{(p)}}{\partial\alpha} \mathrm{e}^{-(t-t')/\tau^{(p)}} H(t-t')\, \dot{\tilde{\epsilon}}^{\dagger}_{ij}(t)\, \delta\alpha\, \mathrm{d}t . \end{aligned} \tag{A5}$$

Substituting the adjoint memory variables $M^{(p)\,\dagger}_{kl}$, defined in (26), we can simplify (A5) into

$$\int_{-\infty}^{\infty} \tilde{\epsilon}^{\dagger}_{ij}(t)\, \delta\dot{\mu}(t-t')\, \mathrm{d}t = -\mu^r\, Q_{0\,\mu}^{-1} \sum_{p=1}^{N} \frac{\partial D^{(p)}}{\partial\alpha} \frac{D^{(p)}}{\tau^{(p)}} \tilde{M}^{(p)\,\dagger}_{ij}(t')\, \delta\alpha . \tag{A6}$$

Combining eqs (A2) with (A6) we can write the variation of the measurement functional $\delta\chi$ in terms of a volumetric Fréchet or sensitivity kernel:

$$\delta\chi = \int_{V} K_{\alpha}(\mathbf{x})\, \delta \ln\alpha(\mathbf{x})\, \mathrm{d}\mathbf{x} , \tag{A7}$$

where the kernel K_α is given in terms of the forward strain deviator $\tilde{\epsilon}_{ij}$ and the deviator of the adjoint memory variables, $\tilde{M}_{p,ij}$:

$$K_{\alpha} = -2\mu^r \alpha\, Q_{0\,\mu}^{-1} \sum_{p=1}^{N} \frac{\tau^{(p)}}{D^{(p)}} \frac{\partial D^{(p)}}{\partial\alpha} \int_{-\infty}^{\infty} \tilde{M}^{(p)\,\dagger}_{ij} \tilde{\epsilon}_{ij}\, \mathrm{d}t . \tag{A8}$$

This proofs eq. (37).

A2 Bulk attenuation

For variations in the viscoelastic properties related to the bulk modulus κ, the variation of the elastic tensor C_{ijkl} condenses to $\delta C_{ijkl} = \delta\kappa$. The variation of the measurement functional χ can then be written in terms of the traces ϵ_{kk} and $\epsilon^{\dagger}_{kk}$ of the forward and adjoint strain tensors:

$$\delta\chi = \int_{-\infty}^{\infty} \int_{V} \left[\int_{-\infty}^{\infty} \epsilon^{\dagger}_{kk}(t)\, \delta\dot{\mu}(t-t')\, \mathrm{d}t \right] \epsilon_{kk}(t')\, \mathrm{d}\mathbf{x}\, \mathrm{d}t' . \tag{A9}$$

Following exactly the same steps as in Section A1, we transform (A9) into

$$\delta\chi = \int_{V} K_{\alpha}(\mathbf{x})\, \delta \ln\alpha(\mathbf{x})\, \mathrm{d}\mathbf{x} , \tag{A10}$$

with the Fréchet kernel

$$K_{\alpha} = -\kappa^r \alpha\, Q_{0\,\kappa}^{-1} \sum_{p=1}^{N} \frac{\tau^{(p)}}{D^{(p)}} \frac{\partial D^{(p)}}{\partial\alpha} \int_{-\infty}^{\infty} M^{(p)\,\dagger}_{kk} \epsilon_{kk}\, \mathrm{d}t . \tag{A11}$$

This is the result previously stated without proof in eq. (42).